Geophysical Research Letters

RESEARCH LETTER
10.1029/2024GL110443

Effect of Regional Anthropogenic Aerosols on Tropical Cyclone Frequency of Occurrence

Hiroyuki Murakami[1]

[1]National Oceanic and Atmospheric Administration/Geophysical Fluid Dynamics Laboratory, Princeton, NJ, USA

Key Points:

- Aerosol reductions in Europe and the U.S. may decrease tropical cyclones in the South Indian Ocean and South Pacific, respectively
- Elevated aerosols from India since 1980 might notably decrease Western North Pacific tropical cyclones
- Projected decreases in frequency of storm occurrence across the tropics due to rising greenhouse gases rather than aerosol changes

Supporting Information:

Supporting Information may be found in the online version of this article.

Correspondence to:

H. Murakami,
hir.murakami@gmail.com

Citation:

Murakami, H. (2024). Effect of regional anthropogenic aerosols on tropical cyclone frequency of occurrence. *Geophysical Research Letters*, *51*, e2024GL110443. https://doi.org/10.1029/2024GL110443

Received 23 MAY 2024
Accepted 26 SEP 2024

Author Contribution:

Conceptualization: Hiroyuki Murakami
Data curation: Hiroyuki Murakami
Formal analysis: Hiroyuki Murakami
Funding acquisition: Hiroyuki Murakami
Investigation: Hiroyuki Murakami
Methodology: Hiroyuki Murakami
Project administration: Hiroyuki Murakami
Resources: Hiroyuki Murakami
Software: Hiroyuki Murakami
Supervision: Hiroyuki Murakami
Validation: Hiroyuki Murakami
Visualization: Hiroyuki Murakami
Writing – original draft: Hiroyuki Murakami
Writing – review & editing: Hiroyuki Murakami

Abstract Previous studies have highlighted the distinct impacts of anthropogenic aerosols from the Western and Eastern Hemispheres on past multi-decadal changes in tropical cyclone frequency of occurrence (TCF). However, the detailed effect of subregional aerosol variations remained unclear. Using idealized simulations with a dynamical climate model, this study reveals that reduced aerosol emissions from Europe and the U.S. since 1980 may have equally contributed to increased TCF over the North Atlantic, with Europe playing a major role in the decreased TCF in the South Indian Ocean and the U.S. contributing to the decrease in TCF in the South Pacific. Additionally, increased aerosol emissions from India since 1980 may have played a major role in decreasing TCF over the western North Pacific compared to increased emissions from China. TCFs are projected to decrease for most global tropics toward the end of this century due to the dominant effect of increasing greenhouse gases.

Plain Language Summary Since 1980, human-made aerosol emissions have decreased in Europe and the U.S. but increased in China and India. This study uses a climate model to explore how regional aerosol changes affect global tropical cyclones. Findings reveal that reduced aerosols from Europe and the U.S. decreased cyclones in the South Indian Ocean and South Pacific, respectively. In contrast, increased aerosols from India decreased tropical cyclones in the western North Pacific more significantly compared to increased aerosols from China. Reduced aerosols from Europe and the U.S. increased tropical cyclones in the North Atlantic to a similar extent. The model projects fewer global cyclones by the end of this century due to rising greenhouse gases, with Europe's and U.S.'s aerosols remaining low and India's increasing. In essence, changing patterns in aerosols and greenhouse gases contribute to shaping the spatial patterns of tropical cyclones.

1. Introduction

Assessing the impact of anthropogenic climate changes on tropical cyclone (TC) activity is of notable scientific and public interest. While many studies focused on projecting changes in TC activity under a warming climate in the future (Camargo et al., 2023; Knutson et al., 2020), it remains challenging to discern whether climatic changes in TC activity have already emerged on a global scale in the past (Knutson et al., 2019). This challenge is partially attributed to the complex nature of the effect of decadal natural variability on TC activity, which may be large compared to the impact of anthropogenic forcing, such as greenhouse gases and anthropogenic aerosols, making the anthropogenic influence difficult to detect. Additionally, the challenge arises from the limitations of reliable long-term observation records for global TCs for identifying the emergence of possible long-term climate changes or trends in global TC activity.

Despite the challenges, Murakami et al. (2020) focused on the global spatial pattern of the trend in TC density, or, in other words, TC frequency of occurrence (TCF, see Section 2.3 for the definition). Using climate models, they revealed that the observed trend in global TCF since 1980 cannot be explained without the influence of external forcings such as greenhouse gases, anthropogenic aerosols, and volcanic eruptions. Additionally, Murakami (2022) and Wang et al. (2023) highlighted the substantial influence of anthropogenic aerosols on the trends in global TCF since 1980. Past studies have reported the impact of local changes in anthropogenic aerosols on local TC activity (e.g., Dunstone et al., 2013; Evan et al., 2011; Mann & Emanuel, 2006; Takahashi et al., 2017). However, Murakami (2022) revealed that anthropogenic aerosols could affect remote TC activity globally. For example, decreased anthropogenic aerosols from the Western Hemisphere (i.e., Europe and the U.S.) could decrease TCF over the open oceans in the Southern Hemisphere and increase TCF over the North Atlantic since 1980. Murakami (2022) also found that increased aerosol emissions from the Eastern Hemisphere (i.e., India and China) could decrease TCF over the tropical western North Pacific since 1980. While Murakami (2022) addressed

the effect of aerosol changes from the relatively large domains of the Western Hemisphere and Eastern Hemisphere on global TCF, it remains an open question to what extent aerosol changes from individual subregions, such as Europe, the U.S., China, and India, could have separately influence global TCF in the past decades.

TCF has increased in the North Atlantic since 1980, which might have been partially caused by decreasing aerosol emissions from Europe and the U.S. However, Murakami et al. (2020) projected a decrease in TCF toward the end of the 21st century due to a dominant effect of greenhouse gases, along with the anticipated unchanged anthropogenic aerosol emissions from Europe and the U.S. Meanwhile, as revealed later, emissions of anthropogenic aerosols from India are expected to increase toward the mid-21st century, raising an open question regarding how TCF would change in the western North Pacific in relation to changes in emissions of anthropogenic aerosols and greenhouse gases.

In this study, we extended the experiments conducted by Murakami et al. (2020) and Murakami (2022), including additional experiments forced by the changes in aerosol emissions only from Europe, the U.S., China, and India. We also explored projected changes in TCFs in a few global subregions under different future scenarios where anticipated changes in emissions of greenhouse gases and anthropogenic aerosols differ. Section 2 provides descriptions of data, a climate model, and experiments. Section 3 presents the results, and finally, Section 5 concludes the study and discussion.

2. Data and Methods

2.1. Observational Datasets

We utilize observed TC data from 1980 to 2020, obtained from the International Best Track Archive for Climate Stewardship (IBTrACS v04r00; Knapp et al., 2010). Specifically, we use a compilation from the National Hurricane Center (NHC) and Joint Typhoon Warning Center (JTWC), identified by the flag 'usa' in the IBTrACS dataset.

2.2. Model and Experiments

Consistent with prior research (Murakami, 2022; Murakami et al., 2020; Wang et al., 2023), we employed the Geophysical Fluid Dynamics Laboratory (GFDL) Seamless System for Prediction and Earth System Research (SPEAR, Delworth et al., 2020) for climate model simulations. The atmospheric and land surface components feature a horizontal resolution of approximately 50 km, while the ocean and ice components use a $1° \times 1°$ mesh. SPEAR simulates the mass distribution of five aerosol types: sulfates, dust, black carbon, organic carbon, and sea salt. Aerosol concentrations in the model are determined by emissions, chemical production for sulfate and secondary organics, dry and wet deposition, advection-based transport, and dry and wet convection. SPEAR also incorporates physical processes capturing the interactions between aerosols, clouds, and convection, known as aerosol indirect effects (Zhao et al., 2018).

As in Murakami (2022), aerosol sensitivity climate simulations were conducted using SPEAR by prescribing various spatial patterns of emissions of anthropogenic aerosols. The top half of Table 1 summarizes the sensitivity experiments. These are referred to as long-term fixed-forcing climate simulations. In these experiments, the solar constant and all anthropogenic forcings, excluding anthropogenic aerosols, were fixed at the year 2000 level to represent the median conditions of the 1980–2020 period. The seven experiments varied in the prescribed emissions of anthropogenic aerosols, including sulfur dioxide, sulfates, black carbon, and organic carbon emissions related to human activity.

The CNTL experiment represents idealized climate conditions for 1980–2000, where the mean emissions of anthropogenic aerosols over the period 1980–2000 were prescribed. W21 is identical to CNTL, except that the 2001–2020 mean emissions of anthropogenic aerosols were prescribed over Europe and the U.S., while the rest of the world remained unchanged from CNTL. The difference between W21 and CNTL represents the impact of changes in anthropogenic aerosol emissions only from Europe and the U.S. Other idealized experiments—USA21, EURO21, IP21, CHINA21, and INDIA21—were also carried out. These experiments are like W21, except that only the changes in aerosol emissions from the U.S., Europe, China and India, China, and India were separately included, respectively.

Table 1
Experimental Settings

Aerosol sensitivity experiments				
Name	Prescribed emissions of anthropogenic aerosols (AA)	Other external forcing	Simulation years	Ensemble members
CNTL	1980–2000 mean	Fixed level at 2000	300	1
W21	As in CNTL, but with 2001–2020 mean AA emissions over Europe and the U.S.			
USA21	As in CNTL, but with 2001–2020 mean AA emissions over the U.S.			
EURO21	As in CNTL, but with 2001–2020 mean AA emissions over Europe			
IP21	As in CNTL, but with 2001–2020 mean AA emissions over India and China			
CHINA21	As in CNTL, but with 2001–2020 mean AA emissions over China			
INDIA21	As in CNTL, but with 2001–2020 mean AA emissions over India			
Large-ensemble experiments				
Name	Prescribed anthropogenic forcings	Volcanic forcing	Simulation period	Ensemble members
Hist	Time-varying during the historical period	Yes	1921–2014	30
SSP119	Time-varying under the SSP1-1.9 scenario	No	2015–2100	
SSP245	Time-varying under the SSP2-4.5 scenario	No	2015–2100	
SSP370	Time-varying under the SSP3-7.5 scenario	No	2015–2100	
SSP534OS	Time-varying under the SSP5-3.4OS scenario	No	2015–2100	
SSP585	Time-varying under the SSP5-8.5 scenario	No	2015–2100	

Note: Using SPEAR, two types of experiments, namely aerosol sensitivity experiments and large-ensemble experiments, were conducted. For aerosol sensitivity experiments, the table includes experiment names, prescribed emissions of anthropogenic aerosols, prescribed level of other external forcings (e.g., greenhouse gases, ozone, and solar constant), the number of simulation years, and the number of ensemble members. For large-ensemble experiments, the table covers experiment names, prescribed anthropogenic forcings (e.g., greenhouse gases, anthropogenic aerosols, and ozone), the presence or absence of volcanic forcing, and the number of ensemble members.

The simulation length is 310 years, with the first 10 years disregarded as the spin-up period, and the simulation outputs from the remaining 300 years were evaluated. A novelty relative to Murakami (2022) is the conduct of new experiments (i.e., USA21, EURO21, CHINA21, and INDIA21) with a longer simulation duration of 300 years. Hereafter, δ represents the difference from CNTL (e.g., δW21), indicating the impact of the specified local aerosol emission changes in the model experiments.

To project TCF globally in the future, we conducted initial-condition large-ensemble experiments using SPEAR. The bottom half of Table 1 provides a summary of the large-ensemble experiments. Detailed descriptions of these experiments can be found in Delworth et al. (2020), Murakami et al. (2020) and Wang et al. (2023). In short, the historical external forcing was prescribed for 1921–2014 in the historical (i.e., Hist) experiment, followed by the Shared Socioeconomic Pathway after 2015 under various future scenarios: SSP1-1.9, SSP2-4.5, SSP3-7.5, SSP5-3.4OS, and SSP5-8.5. To clarify, the numbers in the SSP names (e.g., 1.9 and 8.5) refer to the radiative forcing levels in watts per square meter (W m^2) by the year 2100. The SSP5-3.4OS scenario is an "overshoot" scenario, which initially follows a high-emission pathway like SSP5-8.5 but includes aggressive mitigation efforts later in the century to reduce radiative forcing to 3.4 W m^2 by 2100. The prescribed anthropogenic forcing includes greenhouse gases, anthropogenic aerosols, and ozone. Volcanic forcing was only prescribed before 2006 in Hist, with no volcano eruption assumed for future scenarios. There are 30 ensemble members.

2.3. TC Detection Method

Model-simulated TCs were directly diagnosed from 6 hr outputs using the scheme documented in Murakami et al. (2015) and Harris et al. (2016). A TC must maintain warm core (i.e., 1 K) and wind speed (i.e., 15.75 m s^{-1}) criteria for at least 36 consecutive hours.

Consistent with Murakami et al. (2020), Murakami (2022), and Wang et al. (2023), TC positions were counted every 6 hr over each 5° × 5° grid box globally. The total count for each grid box was defined as the tropical

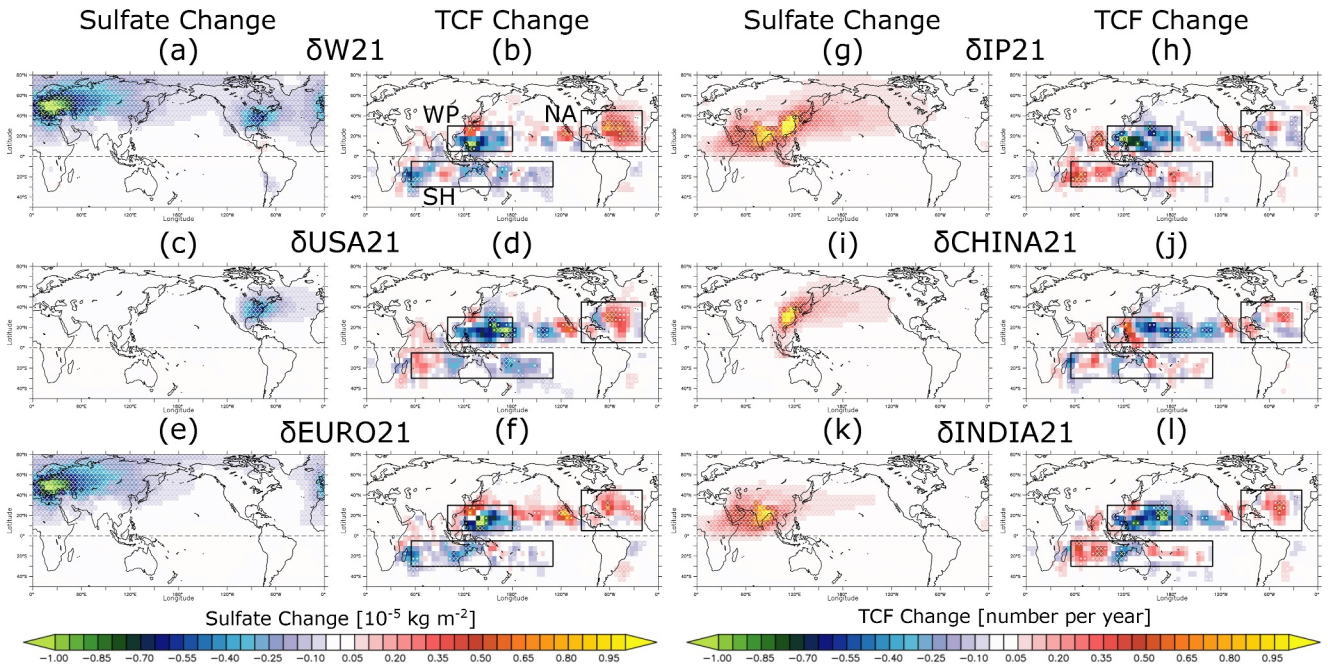

Figure 1. Simulated changes in sulfate and TCF. Panel (a) displays the mean changes in simulated sulfate, while panel (b) depicts the corresponding change in TCF between W21 and CNTL (δWP21). Panels (c), (d), (e), (f), (g), (h), (i), (j), and (k, l) follow a similar format, representing δUSA21, δEURO21, δIP21, δCHINA21, and δINDIA21, respectively. Note that sulfate aerosols are just one type of aerosol included in the experiments, along with black and organic carbon. White crosses (dots) indicate locations where the difference over the grid cell is statistically significant at the 95% (90%) level, as determined by the bootstrap method. The units are 10^{-5} kg m^{-2} for sulfate and number per year per grid for TCF. Rectangles in (b) represent the WP, NA, and SH subdomains as defined in this study.

cyclone frequency of occurrence (i.e., TCF). The TCF fields were further smoothed using a nine-point moving average weighted by distance from the center of the grid box.

2.4. Statistical Significance Test

We employed the bootstrap method proposed by Murakami et al. (2013) to evaluate the statistical significance of the mean difference between the experiments. Two tested populations were resampled in pairs 2,000 times. Subsequently, the difference in the means for each pair was calculated, generating a new distribution with 2,000 samples. The confidence intervals of 90%, 95%, and 99% were obtained from this distribution and compared with the original mean difference.

3. Results

3.1. Changes in TC Spatial Distributions

Figure 1 illustrates the simulated spatial pattern of changes in sulfates and TCF relative to CNTL, while Table 2 presents the total changes in TCF over the tropical western North Pacific (WP), North Atlantic (NA), and open oceans in the Southern Hemisphere (SH), which are the focal regions discussed in Murakami (2022) (defined as the rectangles in Figure 1b). Consistent with Murakami (2022), δW21 reveals statistically significant increases in TCF over the NA and decreases in TCF over the SH (Figures 1b and Table 2). A comparison between δUSA21 and δEURO21, using δW21 as a reference, provides insights into which of the aerosol decreases from the U.S. or Europe is more influential for the TCF changes identified in δW21. Both δUSA21 and δEURO21 exhibit increased TCF in the NA with a similar amplitude, although these increases are not statistically significant (Table 2). This suggests that the significant rise in TCF in the NA by δW21 could partially result from the combined effects of decreased aerosols from Europe and the U.S., both exerting similar impacts. Statistically significant decreases in SH TCF are observed in both δUSA21 and δEURO21, with δEURO21 indicating larger decreases compared to δUSA21 (Table 2). Specifically, the spatial patterns of TCF changes indicate that δEURO21 leads to more pronounced TCF decreases in the South Indian Ocean (Figure 1f), whereas δUSA21 exhibits greater reductions in the South Pacific Ocean (Figure 1d). It is noteworthy that the results are nonlinear;

Table 2
Observed and Simulated Fractional Changes in TCF

	Period or difference	Fractional difference (p-value)		
		WP	NA	SH
Observations	2001–2020 minus 1980–2000	***−22.3***% (0.03)	***30.6***% (0.01)	***−34.5***% (0.00)
δ W21	W21 minus CNTL	−2.1% (0.18)	***7.6***% (0.00)	***−4.3***% (0.02)
δ USA21	USA21 minus CNTL	***−3.6***% (0.02)	3.2% (0.21)	*−2.9*% (0.09)
δ EURO21	EURO21 minus CNTL	−1.8% (0.23)	3.6% (0.16)	***−4.1***% (0.02)
δ IP21	IP21 minus CNTL	***−3.3***% (0.04)	−1.2% (0.64)	2.4% (0.16)
δ CHINA21	CHINA21 minus CNTL	−0.9% (0.58)	0.8% (0.76)	−0.5% (0.77)
δ INDIA21	INDIA21 minus CNTL	***−3.2***% (0.04)	2.8% (0.26)	1.3% (0.45)

Note: The computations were conducted over the domains of the WP, NA, and SH, represented by the black rectangles in Figure 1b. Bold (italic) numbers highlight changes that are statistically significant at the 95% (90%) confidence level, determined through a bootstrap method. Numbers in parentheses denote the associated p-values.

for instance, the addition of δUSA21 to δEURO21 does not consistently result in δW21 (Table 2). Nonlinearity is also evident in the WP. Although the cause of the nonlinearity is still unclear, some studies have reported the existence of nonlinearity in the response of large-scale circulations to changes in regional aerosols and CO_2 (Deng et al., 2019; Deser et al., 2020). Note that the differences in the magnitude of changes between observations and simulations are discussed in Murakami (2022).

In accordance with Murakami (2022), δIP21 demonstrates statistically significant decreases in TCF in the WP (Figures 1h and Table 2). A comparison between δCHINA21 and δINDIA21, using δIP21 as a reference, reveals that δINDIA21 is the primary contributor to the decreases in TCF in the WP (Figures 1k and 1l, Table 2). Although δCHINA21 results in a slight decrease in TCF in the WP, this decrease is not statistically significant (Figures 1j and Table 2). Examining the spatial pattern of TCF changes, δCHINA21 displays a dipole pattern within the WP domain (Figure 1j), while δINDIA21 exhibits an overall decrease in the WP (Figure 1l), mirroring the pattern observed in δIP21 (Figure 1h).

3.2. Changes in Large-Scale Environment

Murakami (2022) identified significant changes in the large-scale environment induced by aerosol changes, which are crucial in modulating TCF across three subdomains. Specifically, the reduction of aerosols from Europe and the U.S. (i.e., δW21) led to the weakening of the subtropical jet in the Northern Hemisphere due to a reduced meridional temperature gradient. This weakening caused a decrease in vertical wind shear, contributing to an increase in TCF in the NA. Additionally, the decrease in aerosols from Europe and the U.S. led to upper-level tropospheric convergence in the tropical Southern Hemisphere, leading to a subsidence anomaly and reduced TCF in the SH (Figure S1a in Supporting Information S1). Consistent with the earlier study, the hemispheric asymmetry in response to interhemispheric aerosol changes can be explained by anomalous upward motions in the Northern Hemisphere due to tropospheric warming resulting from aerosol reduction from Europe and the U.S. This, in turn, induces subsidence anomalies in the Southern Hemisphere through the Hadley Circulation anomaly (Ramaswamy & Chen, 1997; Ming & Ramaswamy, 2009; Ocko et al., 2014; Figure S1a in Supporting Information S1). Our findings indicate that δEURO21 generally aligns with δW21, displaying divergence anomalies in the Northern Hemisphere and convergence anomalies in the Southern Hemisphere. This creates an unfavorable environment for deep convections and TCF in the SH (Figures S1a and S1c in Supporting Information S1). In contrast, δUSA21 generates zonal wave number 2-like patterns in the divergence wind anomalies (Figure S1b in Supporting Information S1). Specifically, δUSA21 induces convergence anomalies in the South Pacific, resulting in decreased TCF in that region, as illustrated in Figure 1d.

In addition, Murakami (2022) uncovered that the increased aerosols from India and China (i.e., δIP21) may have contributed to the weakening of the Indian summer monsoon and the monsoon trough in the WP due to changes in the thermal contrast between the ocean and land surfaces, leading to a reduction in TCF in the WP (Figure S1d in Supporting Information S1). This weakening of monsoon circulation is likely attributed to the heightened aerosol

levels over South and Southeast Asia, which could cool down the land surface relative to open oceans. This cooling effect results in a diminished thermal contrast between the land surfaces and oceans, as was also highlighted by Bollasina et al. (2011). Our findings reveal that, when compared to δCHINA21, δINDIA21 appears to play a dominant role in weakening the Indian summer monsoon and monsoon trough in the WP (Figures S1e and S1f in Supporting Information S1). These distinct changes in large-scale environments help elucidate why TCF in the WP experiences a more significant decrease by δINDIA21 than by δCHINA21.

3.3. Future Changes in TCF

Projecting future TCF poses challenges due to uncertainties in future emission scenarios and model uncertainties in sea surface temperature (SST) spatial variability (e.g., Murakami et al., 2012; Murakami et al., 2020). Specifically, the impact of increased greenhouse gas emissions on TCF differs somewhat from the impact of changes in anthropogenic aerosols on TCF (Murakami et al., 2020). For instance, Murakami et al. (2020) conducted transient +1% CO_2 doubling experiments using SPEAR, revealing significant reductions in TCF globally, especially over the WP, NA, and SH (Figure S2 in Supporting Information S1). Considering that most of the Intergovernmental Panel on Climate Change (IPCC) future emission scenarios project increases in CO_2 emissions (Figure 2e), TCF over the three domains is expected to decrease in the future. However, anticipated changes in anthropogenic aerosol emissions vary among the future scenarios depending on subregions (Figure 2a–2d). Under these scenarios, aerosol emissions from Europe and the U.S. are not expected to differ significantly from the current level (Figures 2a and 2b). This may lead to decreased TCF over the NA and SH in the future due to the dominant role of the CO_2 effect. While aerosol emissions from China are projected to decrease based on the future scenarios (Figure 2c), those from India are expected to increase until the mid-21st century for most of the future scenarios, except for the SSP1-1.9 scenario (Figure 2d). Given the substantial effects of aerosol emissions from India and greenhouse gases on the reduction of TCF over the WP and our model's TCF response to aerosols and greenhouse gases, we anticipate a likely continuing reduction of TCF over the WP in the coming decades.

To further explore these inferences, we conducted 30-member large-ensemble experiments employing anthropogenic forcing under five different future scenarios, which encompass changes in both greenhouse gases and anthropogenic aerosol emissions as boundary forcing (Murakami et al., 2020). Figure 2f–2h depict the time series of total TCF over the three key domains simulated and projected by the ensemble mean of the 30 members. They illustrate significant reductions in TCF toward the end of the 21st century for all three domains under the SSP2-4.5, SSP3-7.0, and SSP5-8.5 scenarios, while the change is relatively small for the SSP1-1.9 scenario. While it appears that increases in greenhouse gases primarily account for the reductions in TCF across the domains, quantifying the relative effect of anthropogenic aerosols on TCF changes compared to the effect of greenhouse gases is challenging based on the information presented in Figure 2.

4. Conclusions

This study builds upon our previous work (Murakami, 2022) by providing further insights into the effects of regional changes in anthropogenic aerosol emissions from four subregions: Europe, the U.S., China, and India, on TCF changes over the three key domains of the NA, WP, and SH. We found that decreases in aerosol emissions from Europe and the U.S. equally contribute to an increase in TCF in the NA. Additionally, the reduction in aerosols from Europe significantly decreases TCF over the South Indian Ocean, while the reduction in aerosols from the U.S. decreases TCF in the South Pacific Ocean. Furthermore, our findings indicate that increased aerosol emissions from India play a substantial role in decreasing TCF in the WP, in contrast to the minimal impact of increased aerosol emissions from China.

These changes in TCF align well with changes in large-scale circulations. Specifically, the reduction in aerosols from Europe potentially creates a hemispheric contrast in anomalies of upper-level divergence winds, manifesting as divergence anomalies in the Northern Hemisphere and convergence anomalies in the Southern Hemisphere. This dynamic leads to suppressed deep convections and TCF in the SH. In contrast, the decreased aerosols from the U.S. generate a zonally oriented alternate anomaly pattern in upper-level divergence winds, resulting in significant convergence anomalies and a reduction of TCF over the South Pacific Ocean.

The impact of increasing aerosols from India or China on TCF changes could be assessed by examining the strength of the summer Indian monsoon and monsoon trough in the WP. Our experiments reveal that the increasing aerosols from India markedly weaken the summer Indian monsoon circulation and monsoon trough in

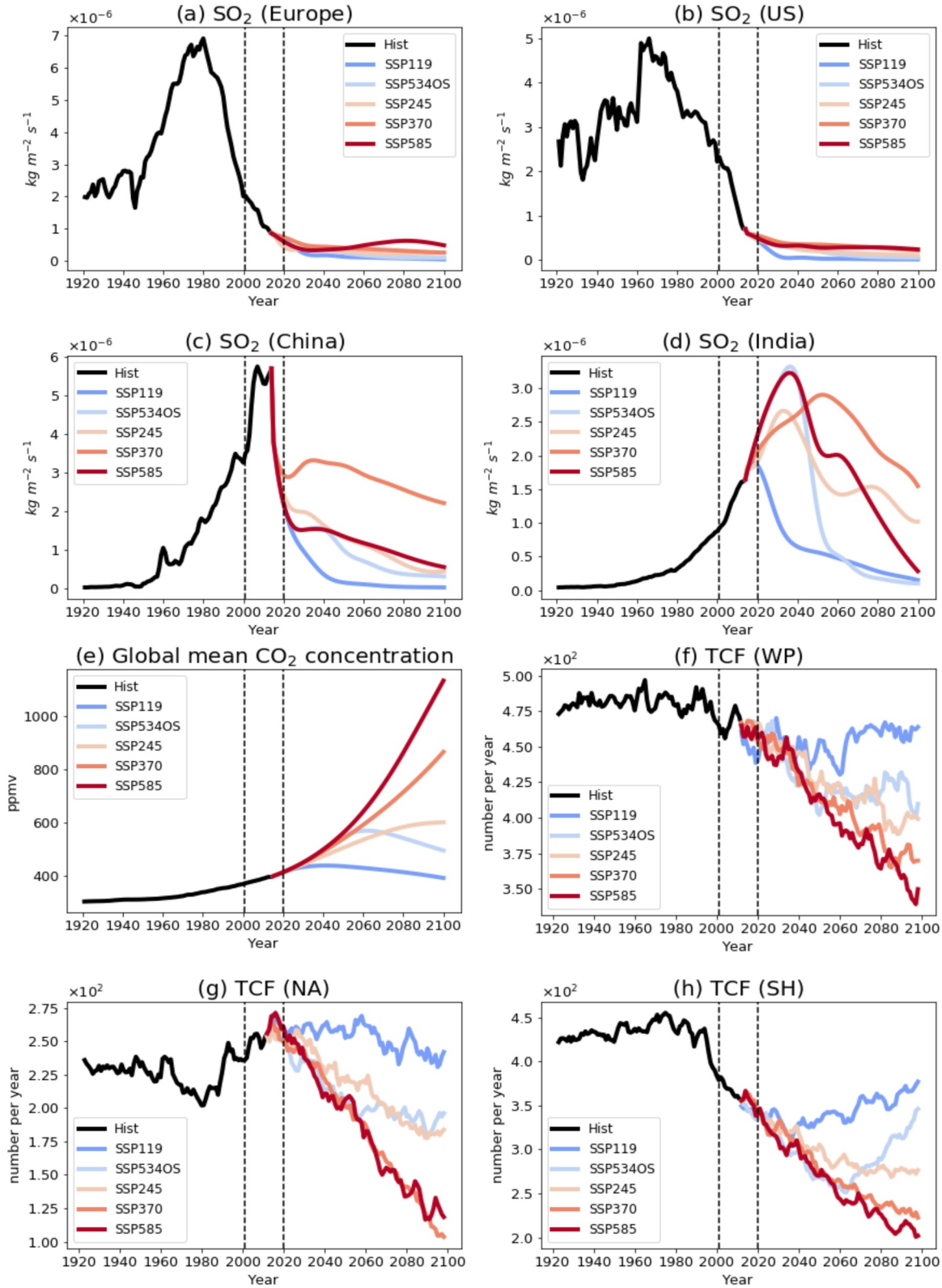

Figure 2. Time series of prescribed emissions of sulfate aerosols, CO_2, and simulated TCF over the subregions by the large-ensemble experiments conducted using SPEAR. (a) The annual mean sulfate aerosol emission from (a) Europe, (b) the U.S., (c) China, and (d) India. Units: 10^{-6} kg m^2. (e) The annual global mean CO_2 concentration. Units: ppmv. (f, g, h) The annual total TCF over the WP, NA, and SH, respectively. Units: number per year. Different colors represent different emission scenarios.

the WP compared to the increasing aerosols from China. This suggests that the potential future changes in aerosol emissions from India constitute an important factor for projecting TCF in the WP.

We conducted projections of TCF over the key domains of the WP, NA, and SH for the future, utilizing large-ensemble simulations conducted by SPEAR under a few different future emission scenarios. SPEAR projected decreases in TCF over the NA and SH toward the end of this century, regardless of the future emission scenarios. This was primarily attributed to sustained low levels of aerosol emissions from Europe and the U.S., coupled with significant increases in greenhouse gas concentrations in the future. Similarly, projected reductions in TCFs were also observed over the WP, driven by the dominant effect of increasing greenhouse gas emissions and the anticipated rise in aerosol emissions from India.

A caveat is that this study relied on a single model. Evaluation and projections using additional models will be crucial to enhance confidence in the reported response of TCF to the anticipated changes in anthropogenic aerosols and greenhouse gases. Quantifying the relative impact of aerosols and greenhouse gases on TCF changes is also important, although it remains a challenging task due to the nonlinearity of the model response of TCF to forcing, as well as the limitations in computational resources for conducting large ensemble experiments with a high-resolution TC-permitting model.

Data Availability Statement

The IBTrACS dataset is online available at the National Centers for Environmental Information website (https://www.ncei.noaa.gov/data/international-best-track-archive-for-climate-stewardship-ibtracs/v04r00/access/csv/ibtracs.ALL.list.v04r00.csv). The SPEAR large-ensemble data for the Hist and SSP585 experiments are online available at https://noaa-gfdl-spear-large-ensembles-pds.s3.amazonaws.com/index.html#SPEAR/GFDL-LARGE-ENSEMBLES/CMIP/NOAA-GFDL/GFDL-SPEAR-MED/. The analyzed data for figures are available via Murakami (2024). These data are freely available. All data needed to evaluate the conclusions in the paper are present in the paper and/or the Supplementary Materials.

Acknowledgments
The author thanks Mr. Thomas Knutson and Dr. V. Ramaswamy for their invaluable suggestions and insightful comments. This study was conducted under award NA18OAR4320123 from the National Oceanic and Atmospheric Administration, U.S. Department of Commerce. The statements, findings, conclusions, and recommendations presented in this study are solely those of the authors and do not necessarily represent the views or official positions of the National Oceanic and Atmospheric Administration or the U.S. Department of Commerce.

References

Bollasina, M. A., Ming, Y., & Ramaswamy, V. (2011). Anthropogenic aerosols and the weakening of the South Asian summer monsoon. *Science*, *334*(6055), 502–505. https://doi.org/10.1126/science.1204994

Camargo, S. J., Murakami, H., Bloemendaal, N., Chand, S., Deshpande, M. S., Dominguez-Sarmiento, C., et al. (2023). An update on the influence of natural climate variability and anthropogenic climate change on tropical cyclones. *Tropical Cyclone Research and Review*, *12*(3), 216–239. https://doi.org/10.1016/j.tcrr.2023.10.001

Delworth, T. L., Cooke, W. F., Adcroft, A., Bushuk, M., Chen, J., Dunne, K. A., et al. (2020). Spear – The next generation GFDL modeling system for seasonal to multidecadal prediction and projection. *Journal of Advances in Modeling Earth Systems*, *12*(3), e2019MS001895. https://doi.org/10.1029/2019MS001895

Deng, J., Dai, A., & Xu, H. (2019). Nonlinear climate responses to increasing CO_2 and anthropogenic aerosols simulated by CESM1. *Journal of Climate*, *33*(1), 281–301. https://doi.org/10.1175/JCLI-D-19-0195.1

Deser, C., Phillips, A. S., Simpson, I. R., Rosenbloom, N., Coleman, D., Lehner, F., et al. (2020). A new CESM1 large ensemble community resource. *Journal of Climate*, *33*(18), 7835–7858. https://doi.org/10.1175/JCLI-D-20-0123.1

Dunstone, N. J., Smith, D. M., Booth, B. B. B., Hermanson, L., & Eade, R. (2013). Anthropogenic aerosol forcing of Atlantic tropical storms. *Nature Geoscience*, *6*(7), 534–539. https://doi.org/10.1038/ngeo1854

Evan, A. T., Kossin, J. P., Chung, C., & Ramanathan, V. (2011). Arabian Sea tropical cyclones intensified by emissions of black carbon and other aerosols. *Nature*, *479*(7371), 94–U119. https://doi.org/10.1038/nature10552

Harris, L. M., Lin, S.-J., & Tu, C. Y. (2016). High resolution climate simulations using GFDL HiRAM with a stretched global grid. *Journal of Climate*, *29*(11), 4293–4314. https://doi.org/10.1175/JCLI-D-15-0389.1

Knapp, K. R., Kruk, M. C., Levinson, D. H., Diamond, H. J., & Neuman, C. J. (2010). The international best track archive for climate stewardship (IBTrACS): Unifying tropical cyclone best track data. *Bulletin America Meteorology Social*, *91*(3), 363–376. https://doi.org/10.1175/2009BAMS2755.1

Knutson, T., Camargo, S. J., Chan, J. C., Emanuel, K., Ho, C., Kossin, J., et al. (2020). Tropical cyclones and climate change assessment: Part II. Projected response to anthropogenic warming. *Bulletin America Meteorology Social*, *101*(3), E303–E322. https://doi.org/10.1175/BAMS-D-18-0194.1

Knutson, T., Camargo, S. J., Chan, J. C. L., Emanuel, K., Ho, C. H., Kossin, J., et al. (2019). Tropical cyclones and climate change assessment: Part I: Detection and attribution. *Bulletin America Meteorology Social*, *100*(10), 1987–2007. https://doi.org/10.1175/BAMS-D-18-0189.1

Mann, M. E., & Emanuel, K. A. (2006). Atlantic hurricane trends linked to climate change. *Eos Transaction of AGU*, *87*(24), 233–241. https://doi.org/10.1029/2006EO240001

Ming, Y., & Ramaswamy, V. (2009). Nonlinear climate and hydrological responses to aerosol effects. *Journal of Climate*, *22*(6), 1329–1339. https://doi.org/10.1175/2008JCLI2362.1

Murakami, H. (2022). Substantial global influence of anthropogenic aerosols on tropical cyclones over the past 40 years. *Science Advances*, *8*(19), eabn9493. https://doi.org/10.1126/sciadv.abn9493

Murakami, H. (2024). Replication data for: Effect of regional anthropogenic aerosols on tropical cyclone frequency of occurrence. https://doi.org/10.7910/DVN/UHABNJ

Murakami, H., Delworth, T. L., Cooke, W. F., Zhao, M., Xiang, B., & Hsu, P.-C. (2020). Detected climatic change in global distribution of tropical cyclones. *Proceedings of the National Academy of Sciences of the United States of America*, *117*(20), 10706–10714. https://doi.org/10.1073/pnas.1922500117

Murakami, H., Mizuta, R., & Shindo, E. (2012). Future changes in tropical cyclone activity projected by multi-physics and multi-SST ensemble experiments using the 60-km-mesh MRI-AGCM. *Climate Dynamics*, *39*(9–10), 2569–2584. https://doi.org/10.1007/s00382-011-1223-x

Murakami, H., Vecchi, G. A., Underwood, S., Delworth, T. L., Wittenberg, A. T., Anderson, W. G., et al. (2015). Simulation and prediction of Category 4 and 5 hurricanes in the high-resolution GFDL HiFLOR coupled climate model. *Journal of Climate*, *28*(23), 9058–9079. https://doi.org/10.1175/JCLI-D-15-0216.1

Murakami, H., Wang, B., Li, T., & Kitoh, A. (2013). Projected increase in tropical cyclones near Hawaii. *Nature Climate Change*, *3*(8), 749–754. https://doi.org/10.1038/nclimate1890

Ocko, I. B., Ramaswamy, V., & Ming, Y. (2014). Contrasting climate responses to the scattering and absorbing features of anthropogenic aerosol forcings. *Journal of Climate*, *27*(14), 5329–5345. https://doi.org/10.1175/JCLI-D-13-00401.1

Ramaswamy, V., & Chen, C.-T. (1997). Climate forcing-response relationships for greenhouse and shortwave radiative perturbations. *Geophysical Research Letters*, *24*(6), 667–670. https://doi.org/10.1029/97GL00253

Takahashi, C., Watanabe, M., & Mori, M. (2017). Significant aerosol influence on the recent decadal decrease in tropical cyclone activity over the western North Pacific. *Geophysical Research Letters*, *44*(18), 9496–9504. https://doi.org/10.1002/2017GL075369

Wang, S., Murakami, H., & Cooke, W. F. (2023). Anthropogenic forcing changes coastal tropical cyclone frequency. *npj Climate and Atmospheric Science*, *6*(1), 187. https://doi.org/10.1038/s41612-023-00516-x

Zhao, M., et al. (2018). The GFDL global atmospheric and land model AM4.0/LM4.0 – Part I: Simulation characteristics with prescribed SSTs. *Journal of Advances in Modeling Earth Systems*, *10*(3), 735–769. https://doi.org/10.1002/2017MS001208